PROCEEDINGS, 44th Workshop on Geothermal Reservoir Engineering
Stanford University, Stanford, California, February 11-13, 2019
SGP-TR-214

Transient Thermoelectric Generation in Oil Wells Under Transient Production

Kai Wang and Xingru Wu

Mewbourne School of Petroleum and Geological Engineering, University of Oklahoma, Norman, OK, USA, 73019

Kai.Wang@ou.edu

Keywords: Heat Transfer, Thermoelectric Technology, Oilfield Geothermal, Numerical Simulation

ABSTRACT

Thermoelectric technology can directly transfer heat into electricity by Seebeck effect with advantages of reliability, compactness and environmental friendliness. Thermoelectric technology is applicable in a large temperature range, and it could be a solution to unlock the potential of low temperature geothermal resources from oil wells. Methods of downhole geothermal power generation using thermoelectric technology in high water-cut wells have been recently proposed to capture the geothermal energy of produced fluids and directly transfer to electricity in the wellbore. Such method could eliminate the dependence on power plant and increase the number of oil wells qualified for geothermal production. Previous studies demonstrated the thermoelectric performance in oil wells under constant production rate, which is not always true in real-world setting.

To fully illustrate the technical feasibility of downhole power generation methods, we studied the transient thermoelectric power generations under varying production rates. A mathematical model is developed to account for the unsteady state heat transfer in the wellbore and surrounding formations, and it is numerically solved using implicit finite-difference method. The temperature profile along the wellbore at any specific time during production could be computed by such model. To accurately characterize the temperature profile and subsequent power generation during oil production, the effective thermal conductivity of thermoelectric generator is included into the numerical model to account for the joule heating generated from thermal-electricity conversion.

The model is validated with other models in the literature and showed good agreement. A case study in North Dakota was conducted to highlight the effect of transient heat transfer on thermoelectric power generations. This study could improve the accuracy of temperature profile and power generation calculations. It could help the operators properly evaluate a hydrocarbon-geothermal coproduction project under field operational conditions and provide accurate estimation of geothermal production for decision makings.

1. INTRODUCTION

Despite of the fact that fossil fuels are supplying the majority of current global energy demand, geothermal energy has been considered as a promising clean energy to mitigate the global warming and minimize environmental footprints. Besides of traditional geothermal development in high geothermal gradient regions, extracting geothermal energy from oil wells has been drawing increasing attentions. Geothermal resource in oilfield not only features the geothermal intrinsic nature of weather independence, reliability, and environmental friendliness, but also is cost-effective to be developed by using existing oilfield assets and resources. Studies have shown rich geothermal resources stored in hydrocarbon-bearing formations around the world. In active oil and gas development countries, such as USA and China, scholars have demonstrated the promising future of oilfield geothermal resources. As shown in Figure1, Augustine and Falkenstern (2012) illustrated the existences of accessible intermediate temperature geothermal resources (100℃-150℃) in the major oil and gas plays in the United States. Moreover, Tester et al.(2006) reported some wells featured even higher temperatures (150℃-200℃) at the bottomhole depth. Major sedimentary basins in China were also described abundant in geothermal resource, such as Daqing Oilfield, Liaohe Oilfield, and Huabei Oilfield, where the total recoverable geothermal resource is estimated as high as 424 EJ (1EJ=10^{18} J) (Wang et al., 2016).

Compared to traditional geothermal fields, oilfields is capable to offer unique advantages to produce geothermal energy in a reduced cost and low-risk manner through existing assets, adequate data and technical resources (Wang et al., 2018a). In return, geothermal applications of space heating, geothermal waterflooding, oil transportation and power generation could help oilfields reduce operation cost, lengthen economic life and achieve environmental and social benefits. All these intrinsic advantages motivate oil operators to develop geothermal energy using existing assets, and some pilot projects have been conducted in Teapot Dome Oilfield in Wyoming (Reinhardt et al., 2011), Huabei Oilfield in China (Xin et al., 2012), and in Eland-Lodgepole Field in North Dakota (Gosnold et al., 2017). In these practices, fluids produced together with oil are usually separated and pumped to a binary cycle power plant for electricity generation. However, these projects are not widely spread, because there are very limited number of oil wells qualified for geothermal production under such practices, which sets a constraint for a large-scale application of geothermal power generation. The technology of binary power plant always has high requirements on water inlet flow rate and temperature. It is estimated that current technologies typically require a minimal daily flow rate of 15,000 barrels with temperature close to 100°C to efficiently generate electricity (Liu et al., 2015). During oil production, heat is lost to surrounding formation, resulting in a lower temperature at surface, which further reduced the number of wells for power generation. Other problems include that the pre-qualified wells may be located in remote areas with a long distance to transport hot water to power plant, which increases the operation cost and heat loss during transportations.

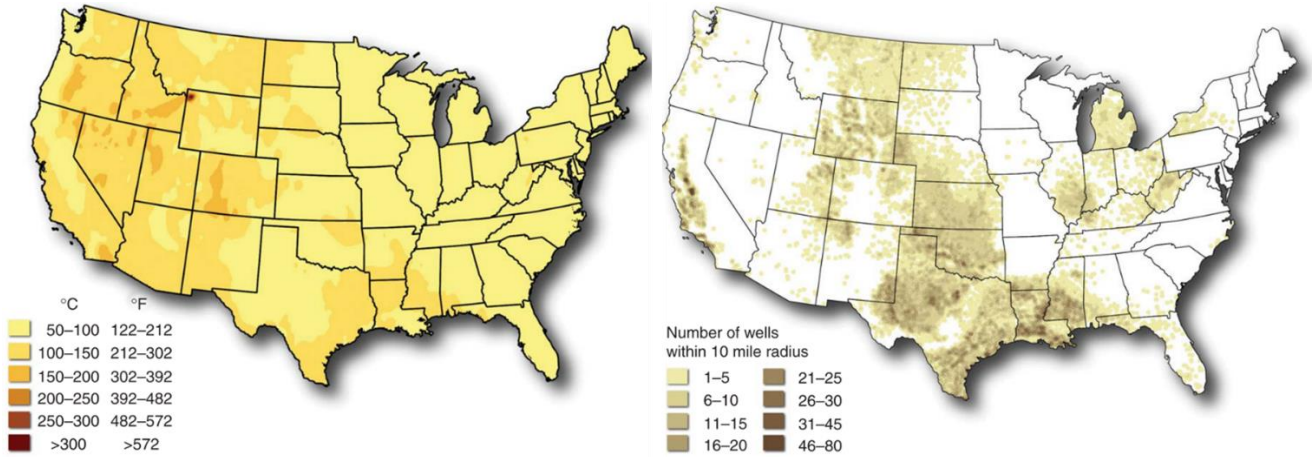

Figure 1: Maps of U.S geothermal temperature at 3500m (left) and well distributions (right) (Augustine and Falkenstern, 2012)

To overcome the limitations of binary power generation, Wang et al. (2018b) introduced thermoelectric technology for geothermal application and proposed an innovative design of downhole power generation from a producing oil well. As described by Wang et al.(2018b), geothermal energy of the produced water is captured and converted to electricity in the wellbore through the pre-installed thermoelectric generators (TEG) on the tubing, instead of heat-electricity conversion in binary power plant. Such method is considered as promising because it could eliminate the dependence on binary power plant and increase the number of oil wells technically qualified for geothermal production. Furthermore, downhole power generation is duplicable in different types of oil wells by incorporating TEG for customized applications for both vertical and horizontal wells (Wang and Wu, 2018). The authors also illustrate the technical viability by establishing a steady state heat transfer model to determine the temperature profile and thermoelectric performance. However, in reality, a producing well always exhibits transient temperature behavior induced by transient production rates during the whole life cycle. Therefore, obtaining a better understanding of transient temperature behavior is critical to evaluate the thermoelectric performance in the previously proposed downhole power generation method.

In this paper, to accurately predict the TEG performance and demonstrate the technical feasibility of such downhole power generation design, a coupled transient heat transfer and TEG model is established. The model accounts for the heat conduction and heat convection in both wellbore and surrounding formation under transient flow rates. The model is solved numerically using finite difference method and validated. Using the transient temperature model, temperature profile at any specific time under any desired production schedule could be attained, and consequently, the dynamic performance of TEG under transient temperature is evaluated. It could help the operators appropriately evaluate their existing assets for oil-geothermal coproduction project under field operational conditions and provide accurate estimation of geothermal production for decision makings.

2. DOWNHOLE GEOTHERMAL POWER GENERATION

Thermoelectric power generation is a mature technology that has been applied to harvest industry waste heat for electricity generation (Ji et al., 2012; Kajikawa, 2011; Zhao et al., 2015, 2014). Downhole power generation method integrated TEG devices into wellbore conditions and created temperature differences across the devices for power generation. The detailed working principles and wellbore constructions are described by Wang et al. (2018b) and (Wang and Wu, 2018). The fundamental structure of TEG device and the application of TEG for downhole power generation are shown in following Figure 2 and Figure 3, respectively.

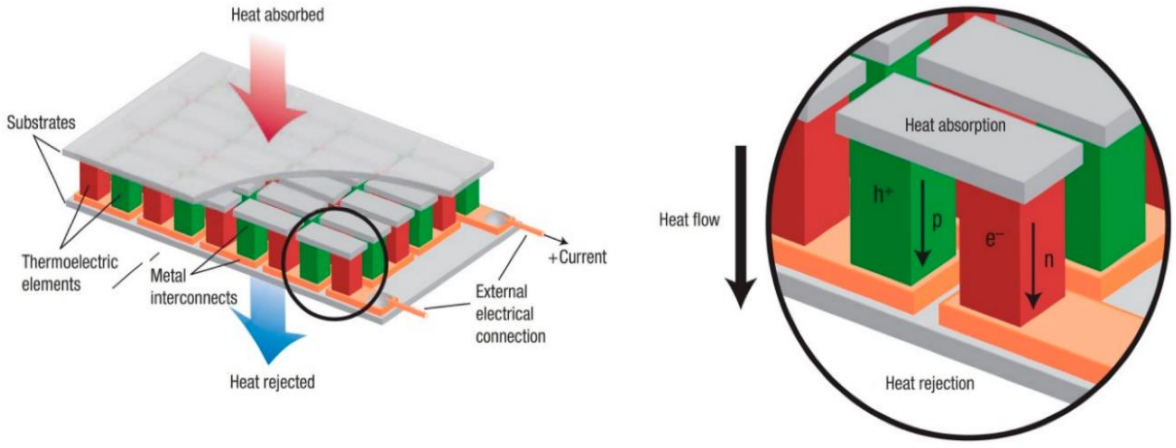

Figure 2: Structure and heat flow in TEG devices (after Snyder and Toberer, 2008)

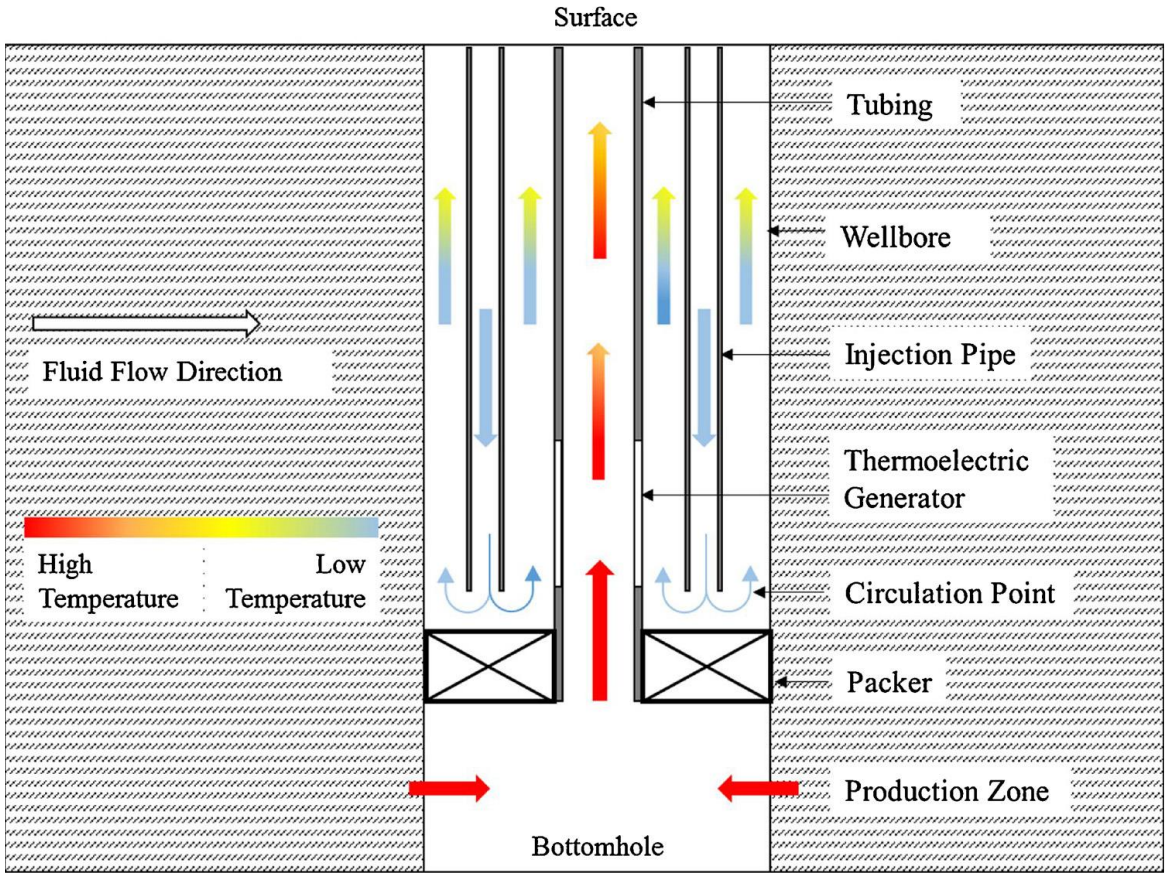

Figure 3: Wellbore constructions for downhole power generation (Wang et al., 2018b)

3. TRANSIENT HEAT TRANSFER MODEL

3.1 Description of Heat Transfer Process

As describe in previous work (Wang et al., 2018b), temperature distribution along the wellbore is obtained by analytical method based on the assumption of constant production rate. However, in reality, oil wells always produce at varying rates, which results in transient temperature profiles. In the configuration of the downhole power generation, the associated heat transfer mainly includes heat transfer in the formation, conduction between formation and wellbore, conduction in pipe walls, convection between fluids and pipe walls, and conduction from hot side of TEG to cold side. To be more specific, as hot fluid produced from the reservoir flow upwards in tubing, heat transfer happens at tubing wall through convection. Convection also occurs in the annulus between injected cold fluid and the contacting tubing/casing walls. On the other hand, the heat transfer inside tubing, casing, cement and formation are dominated by conduction. Heat transfer from hot side to cold side in TEG is also in form of heat conduction. In this model, heat conduction is represented by Fourier's Law and heat convection is characterized by heat transfer coefficient.

3.2 Mathematical Model of Transient Heat Transfer

We setup a 2D radial-vertical cylindrical coordinate to study the heat transfer problem stated above with the following assumptions. 1) The rate of fluid flow is only a function of time. 2) All fluids are assumed to be Newtonian fluid with a constant density and thermal properties. 3) Geothermal gradient in the formation is constant. 4) The Joule-Thompson effect, viscous dissipation and thermal expansion in wellbore are all negligible. 5) Thermoelectric material used in this study is assumed to be homogenous and isotropic with constant values of properties. 6) Heat transfer in TEG is considered as 1-D heat conduction from hot side to cold side. The wellbore geometry is divided into different regions in radial direction as shown in Figure 4. Staring from the center of the wellbore to formation, the physical meaning of each region is tubing, tubing wall, annulus, casing wall, cement and formation, respectively (Table 1).

The fluid flow and heat transfer in this model could be expressed by the equation of change in non-isothermal system. For any volume of element in this geometry, the equation of energy conservation could be written as

$$\frac{\partial}{\partial t}\left(\frac{1}{2}\rho v^2+\rho U\right)=-\left(\nabla\cdot\left(\frac{1}{2}\rho v^2+\rho U\right)v\right)-\nabla\cdot q-\nabla\cdot pv-\nabla\cdot(\tau\cdot v)+\rho(v\cdot g) \tag{1}$$

where ρ and v are the density and the velocity of the fluid, respectively. P stands for the pressure, and U represents the internal energy of the fluid per unit mass. g is the acceleration of gravity. Therefore, it is easy to tell that the term on the left side of equation represents the rate of kinetic and internal energy change per volume, and the terms on the right side represents: rate of increase of energy per volume due to convection, rate of energy increase due to molecular transport, rate of work done on the fluid by viscous forces, rate of work done on the fluid by pressure forces, and rate of work done on the fluid by gravitational forces, respectively.

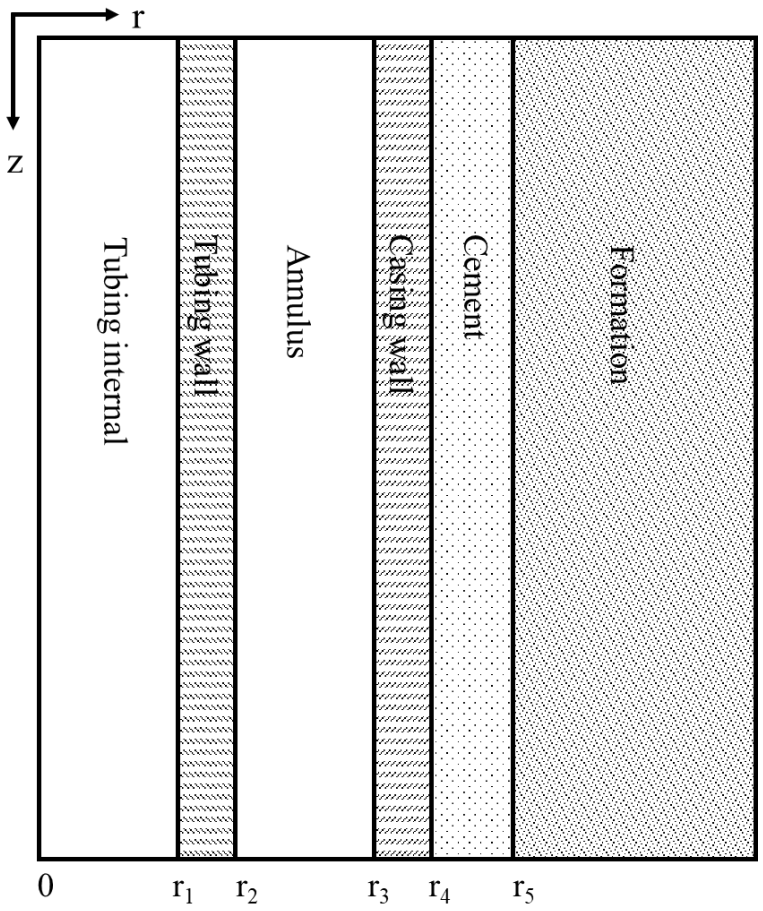

Figure 4: Geometry of the heat transfer model of the wellbore and formation

Table 1: Physical meaning and ranges of each region

Region	Physical meaning	Ranges
1	Tubing internal	$0 < r < r_1$
2	Tubing wall	$r_1 \le r \le r_2$
3	Annulus	$r_2 < r < r_3$
4	Casing wall	$r_3 \le r \le r_4$
5	Cement	$r_4 < r < r_5$
6	Formation	$r \ge r_5$

The equation of mechanical energy change is,

$$\frac{\partial}{\partial t}\left(\frac{1}{2}\rho v^2\right) = -\left(\nabla \cdot \frac{1}{2}\rho v^2 v\right) - \nabla \cdot pv - \nabla \cdot (\tau \cdot v) - (-\tau : \nabla v) + \rho(v \cdot g) \tag{2}$$

Subtract Equation 2 from 1, we could obtain the equation of change for internal energy,

$$\frac{\partial}{\partial t}(\rho U) = -(\nabla \cdot \rho U v) - \nabla \cdot q - \nabla \cdot pv - (\tau : \nabla v) \tag{3}$$

Since flow rate is only time dependent, it can be simplified as,

$$\frac{\partial}{\partial t}(\rho U) = -(\nabla \cdot \rho U v) - \nabla \cdot q - \nabla \cdot pv \tag{4}$$

Heat conduction is modeled by using Fourier's Law, and cast in a cylindrical coordinate as,

$$\rho C_P\left(\frac{\partial T}{\partial t} + v_r\frac{\partial T}{\partial r} + v_z\frac{\partial T}{\partial z}\right) = \frac{k_r}{r}\frac{\partial T}{\partial r} + k_r\frac{\partial^2 T}{\partial r^2} + k_z\frac{\partial^2 T}{\partial z^2} \tag{5}$$

where C_p is the specific thermal capacity of the fluid, k_r is the thermal conductivity in the radial direction and k_z is the thermal conductivity in vertical direction. Therefore, the governing equation in this model is obtained as Eq. (5). The initial condition is set as all the gridblock are at its geothermal temperature, which is a linear relationship with depth. Based on the different heat transfer and fluid flow process in different regions, the governing equation is re-writing to be representative for specific process, and the boundary conditions are also applied in each region.

3.3 Numerical Solution

Finite difference method is applied to discretize the partial differentials implicitly. For space in radial and vertical direction, use *i* and *j* to represent the gridblocks in each direction, respectively. The first order and second order of spatial discretization could be expressed as,

$$\frac{\partial T}{\partial r} = \frac{T_{i+1,j}^{t+\Delta t} - T_{i-1,j}^{t+\Delta t}}{2\Delta r} \tag{6}$$

$$\frac{\partial T}{\partial z} = \frac{T_{i,j+1}^{t+\Delta t} - T_{i,j-1}^{t+\Delta t}}{2\Delta z} \tag{6}$$

$$\frac{\partial^2 T}{\partial r^2} = \frac{T_{i+1,j}^{t+\Delta t} - 2T_{i,j}^{t+\Delta t} + T_{i-1,j}^{t+\Delta t}}{\Delta r^2} \tag{7}$$

$$\frac{\partial^2 T}{\partial z^2} = \frac{T_{i,j+1}^{t+\Delta t} - 2T_{i,j}^{t+\Delta t} + T_{i,j-1}^{t+\Delta t}}{\Delta z^2} \tag{8}$$

Write the time discretization as,

$$\frac{\partial T}{\partial t} = \frac{T_{i,j}^{t+\Delta t} - T_{i,j}^{t}}{\Delta t} \tag{9}$$

And the equations in each region could be expressed as

$$A_{i,j}T_{i,j-1}^{t+\Delta t} + B_{i,j}T_{i,j}^{t+\Delta t} + C_{i,j}T_{i,j+1}^{t+\Delta t} = D_{i,j} \tag{10}$$

Therefore, the temperature profile in each region could be obtained by solving the above equations using tridiagonal matrix algorithm (Thomas algorithm). The simplified governing equations, boundary conditions, overall heat transfer coefficients and effective thermal conductivity of TEG are all expressed in the appendix.

3.4 Effective Thermal Conductivity of TEG

It is worthy to be noticed that, the TEGs are installed on the outer surface of tubing and belong to this region, therefore, the effect of TEG on temperature distribution should be considered in this region. TEG under temperature differences will result in heat conduction from hot side to cold side and Joule heating by heat-electricity conversion. To include these effects into temperature distribution, a parameter named "effective thermal conductivity" of TEG (Baranowski et al., 2013) is introduced to encompass the overall heat transfer phenomena. The effect of TEG on heat transfer could be embodied by replacing the thermal conductivity by the effective thermal conductivity. The expression of effective thermal conductivity is

$$k_{eff} = \frac{kT_h\left(1+zT+\sqrt{zT+1}\right)}{2\left(T_h-T_c\right)}\left[1-\left(\frac{T_h}{T_c}\right)^{\beta}\right] \tag{11}$$

$$\beta = \frac{2-2\sqrt{zT+1}}{zT} \tag{12}$$

where T_h and T_c are the temperature values at hot side and cold side, respectively, and k is the thermal conductivity of the thermoelectric material. zT is the dimensionless figure of merit, standing for the ability of a given material to efficiently produce thermoelectric power as

$$zT = \frac{\alpha^2}{k\sigma}\frac{T_h+T_c}{2} \tag{13}$$

3.5 Model Validations

To validate the transient heat transfer model, two sets of field data are employed to classic Ramey's model (Ramey, 1962) and previously proposed analytical model (Wang et al., 2018b), respectively and compare the results with transient heat transfer model. To conduct the validation with Ramey's model, a case of cold-water injection into a vertical well is studied by applying two models. The well is drilled to 6605 ft, and cased with 7'' 23lb/ft casing. The geothermal gradient of 0.0083°F/ft and the water is injected at 58.5°F. The results comparison is plotted in Figure 5, which indicates a good match of two models.

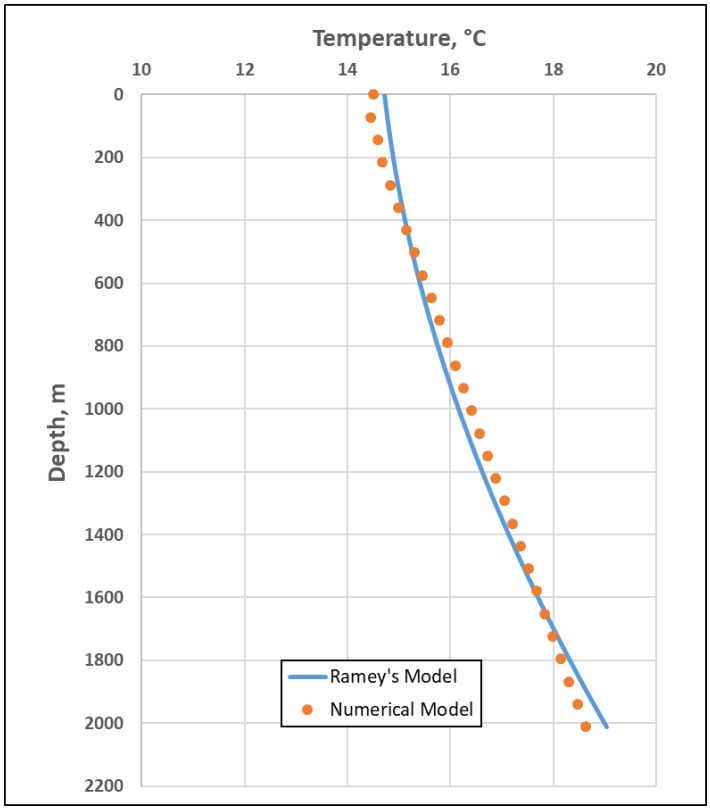

Figure 5: Transient Model Validation with classic Ramey's model

Similarly, based on the downhole construction in Figure 3 and use the data of case study in the previous steady-state case as the basic case, and change the production rate in different time steps (T1, T2 and T3) and compare the temperature history as plotted in Figure 6, which also shows a good match of temperature profile after three time steps and close to steady state temperature profile. Therefore, we validated the numerical transient heat transfer model and it is further applied for case studies to illustrate the improved accuracy in temperature profile modeling and power generation estimation.

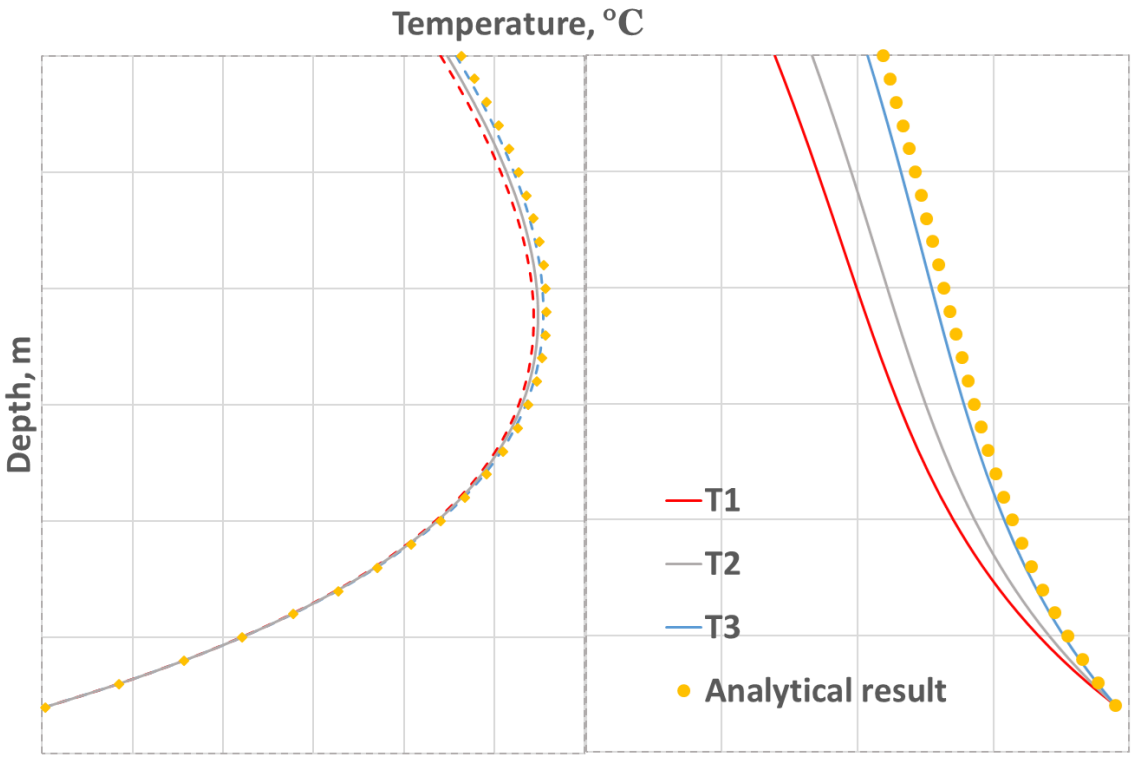

Figure 6: Validation results of numerical model and analytical model

4. CASE STUDY

Eland-Lodgepole Field in North Dakota is used for cast study. It is the one of the most prolific Lower Mississippian Lodgepole mound complex found to date in the Williston Basin, and covers an area of about 6 square miles with cumulative production of more than 29 million barrels of oil since 1993 (Longman and Cumella, 2016). The operators conducted secondary recovery by waterflooding with 12 producing oil wells, 5 injection wells and one disposal well. Average water production is approximately 320 gallons per minute with the temperature close to 100 ºC. Geothermal gradient and surface temperature in this area is recorded as 0.027°C/m and 13°C, respectively (Gosnold et al., 2017). The wellbore is retrofitted according to the downhole power generation design in Figure 3 with the related parameters listed as following Table 4. The well is produced in transient rates due to variations in waterflooding schedule and the production history is also shown as Table 4.

Table 2: Wellbore/ reservoir properties and production schedule in this case study

Wellbore/ reservoir properties			
Tubing OD	3.5 in	Bottomhole depth	9843 ft
Tubing ID	2.992 in	Cold water temperature	15°C
Casing OD	9.625 in	Cold fluid injection rate	60 m^3/d
Casing ID	8.835 in	Water specific heat capacity	4.2 kJ/ (kg K)
Injection pipe OD	1.05 in	Formation thermal conductivity	2.42 W/(mK)
Injection pipe ID	0.824 in	Cement thermal conductivity	6.95 W/(mK)

Production Schedule	
Time, day	Rate, m^3/d
30	145
45	200
45	100

Based on the given information, the numerical transient heat transfer model is applied to the case study and characterize the temperature behavior in different the production schedules. The temperature profile change along the given production time is plotted in Figure 7, and temperature profile of the first 30 days is plotted in Figure 7, respectively.

Considering the temperature change from initial condition to 120 days in Figure 7, the initial produced fluid, which flows upward with the same temperature as the production zone, will heat up the flow pathway and the near-wellbore region by losing heat to the surrounding formation due to temperature difference, which can be easily identified by the change of temperature in the wellbore region as shown in Figure 7-a and 8-b. Meanwhile, to artificially create the temperature difference across the TEG, cold water is injected in the annulus, which results in the low temperature region of the injection pipe in the annulus as shown in the Figure 7-b, 8-c and 8-d. Variations in production rate induced the change of temperature profiles in the wellbore and the surrounding formation. When production rate increased after 30 days, higher flow rate reduced the heat loss from the fluid to the annulus and resulted in the temperature increase in the tubing and temperature decrease in the annulus due to less heat conducted out to heat up the injected fluid. After the production rate drop from 200 m3/day to 100m3/day at 75 days, the lower flow rate allows increased heat conduction to the annulus, and consequently resulted in the temperature decrease in the tubing, indicated by the temperature profile change from Figure 7-c to Figure 7-d.

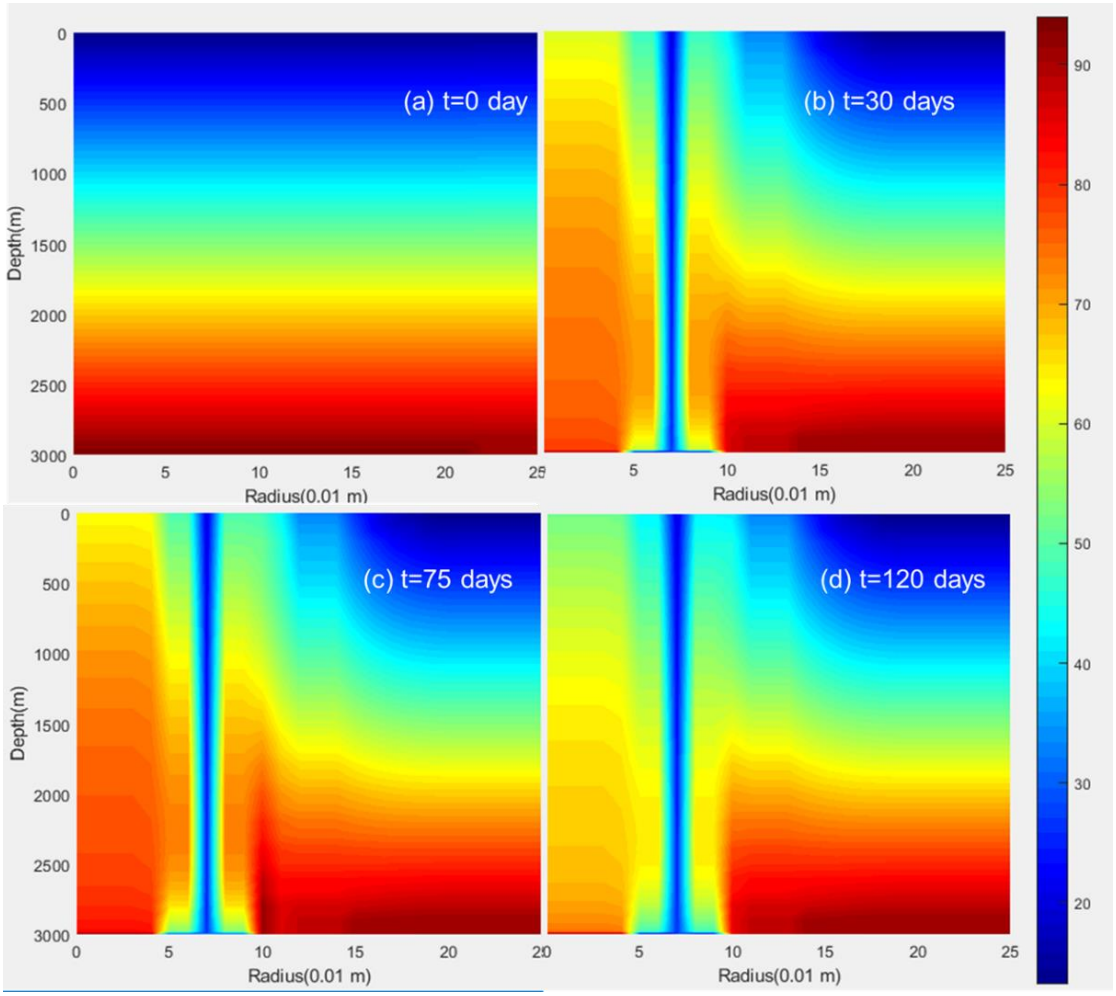

Figure 7: Temperature profile in the wellbore and surrounding formations in given production history

To study the temperature profile in given time, from the Figure 8, we can clearly see the temperature distribution in different physical regions due to downhole power generation construction. In region 1 and region 2, the temperature behavior is same as routine oil production with a temperature drop from bottomhole to surface and slightly temperature drop in tubing wall. In region 3, due to the cold-water injection in the middle of the annulus, which creates a low temperature flow path from top to bottom, the annulus is cooled down compared to the normal oil production. At the bottomhole depth, the maximum temperature difference is created, and it is the place that TEG is installed. The heat conduction from the tubing and the formation will heat up the injected water when it reverses its flow direction towards the surface, therefore, we can see the temperature increase in the lower part of the annulus above the TEG. The temperature behavior in the annulus also caused the temperature distribution changes in the formation, however, under continuous heat conduction supply from nearby formation, the temperature in the formation will reach the equilibrium temperature in certain radial distance, which is affected by the cold-water flow rate.

The transient production rates brought the change of temperature field in the whole wellbore, and consequently altered the temperature gradient across the TEG device as well as the power output. The trainset numerical heat transfer model could generate the temperature data in any given time, which enables the power generation to be simulated in corresponding timesteps and improve the calculation accuracy.

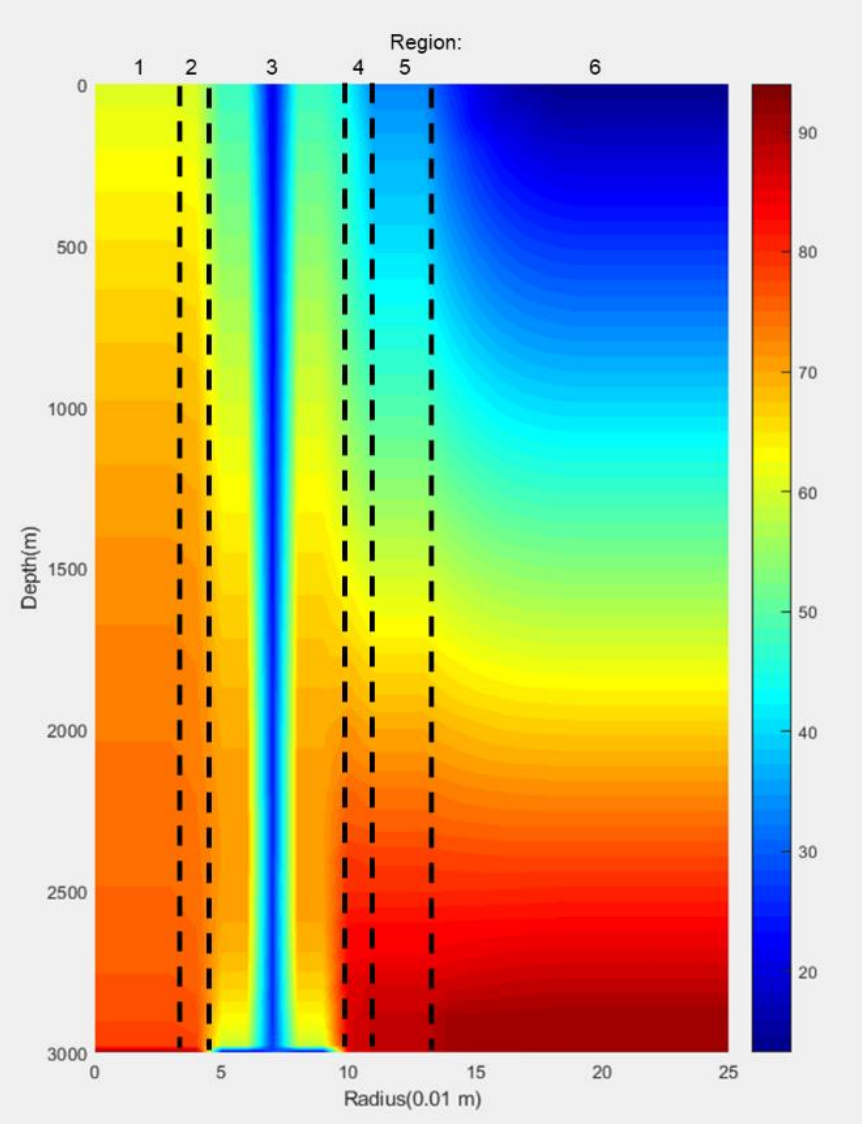

Figure 8: Temperature profile in the wellbore and surrounding formations in the first 30 days

FUTURE WORK

To enhance the geothermal development from oil wells, it is desired to maximum the thermoelectric power generation which is a function of temperature difference and thermoelectric material properties. Previous work and this work are both aiming to maximize and accurately quantify the temperature difference. Part of my future work will be choosing high-performance fluid and optimizing the cold fluid injection pumping schedule to further decreasing the cold side temperature for maximized temperature difference under operational constraints.

Another part of the future work could be focused on optimizing the selections of suitable thermoelectric material based on the given temperature ranges of the well and the project economics. As the evaluation of science and technology in nanomaterials (Cui et al., 2014; Ji et al., 2014; Mamur et al., 2018; Xu et al., 2011), and electronic devices (Fang et al., 2011; Ji et al., 2011; Zhao et al., 2015), it could be expected that geothermal power generation in oil wells will be further enhanced along with the TEG technology development.

CONCLUSIONS

This paper proposed a transient heat transfer model to numerically simulate the temperature distribution in complicated wellbore configurations under variable production rates. Based on the discussions above, following conclusions are drawn as the key findings of the paper.

- The proposed numerical model is capable to account for the fluid flow and heat transfer processes during transient production rate, which enables transient power generation simulation under field operation conditions.
- The numerical model applied the parameter of effective thermal conductivity to include the internal heating during heat-electricity conversion in TEG, and improved the characterizing of temperature behavior.
- The proposed model could benefit the future work on cold fluid selection and injection optimizations by delivering accurate temperature data at any given fluid flow rate.
- This work could provide a reliable method for oil and gas operators to properly forecast the temperature behavior during long-time productions, help them evaluate the oil well geothermal potential, and pinpoint the opportunities to capture the geothermal resource stored in the produced fluids.

REFERENCES

Augustine, C., Falkenstern, D., 2012. An Estimate of the Near-Term Electricity Generation Potential of Co-Produced Water From Active Oil and Gas Wells. SPE J. 36. https://doi.org/10.2118/163142-PA

Baranowski, L.L., Snyder, G.J., Toberer, E.S., 2013. Effective thermal conductivity in thermoelectric materials. J. Appl. Phys. 204904, 1–11. https://doi.org/10.1063/1.4807314

Cui, B., Xu, Y., Ji, G., Wang, H., Zhao, W., Zhai, Y., Li, D., Liu, D., 2014. A single-molecule diode with significant rectification and negative differential resistance behavior. Org. Electron. physics, Mater. Appl. 15, 484–490. https://doi.org/10.1016/j.orgel.2013.11.039

Fang, C., Cui, B., Xu, Y., Ji, G., Liu, D., Xie, S., 2011. Electronic transport properties of carbon chains between Au and Ag electrodes: A first-principles study. Phys. Lett. Sect. A Gen. At. Solid State Phys. 375, 3618–3623. https://doi.org/10.1016/j.physleta.2011.08.032

Gosnold, W., Mann, M., Salehfar, H., 2017. The UND-CLR Binary Geothermal Power Plant. GRC Trans. 41, 1824–1834.

Ji, G., Cui, B., Xu, Y., Fang, C., Zhao, W., Li, D., Liu, D., 2014. Enhanced rectifying performance by asymmetrical gate voltage for BDC20 molecular devices. RSC Adv. 4, 16537. https://doi.org/10.1039/c3ra47408a

Ji, G., Li, D., Fang, C., Xu, Y., Zhai, Y., Cui, B., Liu, D., 2012. Effect of contact interface configuration on electronic transport in (C20)2-based molecular junctions. Phys. Lett. Sect. A Gen. At. Solid State Phys. 376, 773–778. https://doi.org/10.1016/j.physleta.2011.12.025

Ji, G., Zhai, Y., Fang, C., Xu, Y., Cui, B., Liu, D., 2011. The electronic transport properties in C60 molecular devices with different contact distances. Phys. Lett. Sect. A Gen. At. Solid State Phys. 375, 1602–1607. https://doi.org/10.1016/j.physleta.2011.02.058

Kajikawa, T., 2011. Overview of Thermoelectric Power Generation Technologies in Japan.

Liu, X., Gluesenkamp, K., Momen, A., 2015. Overview of Available Low-Temperature / Coproduced Geothermal Resources in the United States and the State of the Art in Utilizing Geothermal Resources for Space Conditioning in Commercial Buildings.

Longman, M.W., Cumella, S.P., 2016. Revisiting the Eland Field Lodgepole Mound Complex (Stark County , North Dakota) Twenty Years after its Discovery. Mt. Geol. 53, 29–70.

Mamur, H., Bhuiyan, M.R.A., Korkmaz, F., Nil, M., 2018. A review on bismuth telluride (Bi2Te3) nanostructure for thermoelectric applications. Renew. Sustain. Energy Rev. 82, 4159–4169. https://doi.org/10.1016/J.RSER.2017.10.112

Ramey, H.J., 1962. Wellbore Heat Transmission. J. Pet. Technol. 14, 427–435. https://doi.org/10.2118/96-PA

Reinhardt, T., Johnson, L.A., Popovich, N., Poplar, N., 2011. Systems for Electrical Power From Coproduced and Low Temperature Geothermal Resources, in: Proceedings of 36th Workshop on Geothermal Reservoir Engineering.

Snyder, G.J., Toberer, E.S., 2008. Complex thermoelectric materials. Nat. Mater. 7, 105–114. https://doi.org/10.1038/nmat2090

Tester, J.W., Anderson, B.J., Batchelor, A.S., Blackwell, D.D., DiPippo, R., 2006. The Future of Geothermal Energy - Impact of Enhanced Geothermal Systems (EGS) on the United States in the 21st Century, Massachusetts Institute of Technology.

Wang, K., Wu, X., 2018. A Design of Downhole Thermoelectric Generation for Horizontal Oil Wells. GRC Trans. 42.

Wang, K., Yuan, B., Ji, G., Wu, X., 2018a. A comprehensive review of geothermal energy extraction and utilization in oilfields. J. Pet. Sci. Eng. 168, 465–477. https://doi.org/10.1016/j.petrol.2018.05.012

Wang, K., Liu, J., Wu, X., 2018b. Downhole geothermal power generation in oil and gas wells. Geothermics 76, 141–148. https://doi.org/10.1016/j.geothermics.2018.07.005

Wang, S., Yan, J., Li, F., Hu, J., Li, K., 2016. Exploitation and utilization of oilfield geothermal resources in China. Energies 9, 1–13. https://doi.org/10.3390/en9100798

Xin, S., Liang, H., Hu, B., Li, K., 2012. A 400 kW Geothermal Power Generator Using Co-Produced Fluids From Huabei Oilfield. GRC Trans. 36.

Xu, Y., Fang, C., Cui, B., Ji, G., Zhai, Y., Liu, D., 2011. Gated electronic currents modulation and designs of logic gates with single molecular field effect transistors. Appl. Phys. Lett. 99, 1–4. https://doi.org/10.1063/1.3615691

Zhao, W., Cui, B., Fang, C., Ji, G., Zhao, J., Kong, X., Zou, D., Jiang, X., Li, D., Liu, D., 2015. Rectification inversion in oxygen substituted graphyne–graphene-based heterojunctions. Phys. Chem. Chem. Phys. 17, 3115–3122. https://doi.org/10.1039/C4CP04859H

Zhao, W., Ji, G., Liu, D., 2014. Contact position and width effect of graphene electrode on the electronic transport properties of dehydrobenzoannulenne molecule under bias. Phys. Lett. A 378, 446–452. https://doi.org/10.1016/J.PHYSLETA.2013.12.006

APPENDIX

Tubing Internal Region

In this region, produced fluid is flowing upward under time-dependent rates and heat loss happens in radial direction by convention at the inner tubing wall. Since the fluid is flowing only in vertical direction without radial flow, the governing equation in region 1 can be written as,

$$\rho_1 C_{P1}\left(\frac{\partial T}{\partial t}+v_z\frac{\partial T}{\partial z}\right)=\frac{k_r}{r}\frac{\partial T_1}{\partial r}+k_r\frac{\partial^2 T_1}{\partial r^2}+k_z\frac{\partial^2 T_1}{\partial z^2} \tag{14}$$

The wellbore is treated as a symmetric geometry and region 1 starts from the center of the wellbore (tubing), which gives no heat flux at the position *r=0*. Heat convention happens at the contacting area of fluid and tubing wall. Therefore, two boundary conditions of region 1 can be expressed as,

$$\left(\frac{\partial T_1}{\partial r}\right)_{r=0}=0 \tag{15}$$

$$-k_1\left(\frac{\partial T_1}{\partial r}\right)_{r=r_1}=h_1\left(T_1-T_2\right) \tag{16}$$

Apply these two boundary conditions and obtain the expressions of A, B, C and D in this region as,

$$A_{1,j}=-v_{1,j}\left(\frac{\Delta t}{2\Delta z_j}\right)-\frac{k_{z1,j}}{\rho_{1,j}C_{p_{1,j}}}\left(\frac{\Delta t}{\Delta z_j^2}\right) \tag{17}$$

$$B_{1,j}=1+\left(\frac{2h_{1,j}}{r_1}+\frac{2k_{z1,j}}{\Delta z_j^2}+\frac{3k_{r1,j}}{r_1^2}\right)\left(\frac{\Delta t}{\rho_{1,j}C_{p_{1,j}}}\right) \tag{18}$$

$$C_{1,j}=v_{1,j}\left(\frac{\Delta t}{2\Delta z_j}\right)-\frac{k_{z1,j}}{\rho_{1,j}C_{p_{1,j}}}\left(\frac{\Delta t}{\Delta z_j^2}\right) \tag{19}$$

$$D_{1,j}=T_{1,j}^t+\left(\frac{2h_{1,j}}{r_i}+\frac{2k_{z1,j}}{\Delta z_j^2}+\frac{3k_{r1,j}}{r_1^2}\right)\left(\frac{\Delta t}{\rho_{1,j}C_{p_{1,j}}}\right)T_{2,j}^t \tag{20}$$

Tubing Wall Region

In this region, there is no fluid flow. Heat conducts through the tubing wall and heat convention happens at the outer with the annulus fluid. Therefore, the governing equation and boundary conditions can be written as follows.

$$\rho_2 C_{P2}\left(\frac{\partial T}{\partial t}\right)=\frac{k_r}{r}\frac{\partial T_2}{\partial r}+k_r\frac{\partial^2 T_2}{\partial r^2}+k_z\frac{\partial^2 T_2}{\partial z^2} \tag{21}$$

$$-k_1\left(\frac{\partial T_1}{\partial r}\right)_{r=r_1}=h_1\left(T_1-T_2\right) \tag{22}$$

$$-k_2\left(\frac{\partial T_2}{\partial r}\right)_{r=r_2}=h_2\left(T_2-T_3\right) \tag{23}$$

Similarly, expressions of A, B, C and D in region 2 can be obtained as,

$$A_{2,j}=-\frac{k_{z,j}}{\rho_{2,j}C_{p_{2,j}}}\left(\frac{\Delta t}{\Delta z_j^2}\right) \tag{24}$$

$$B_{2,j}=1+\left[\frac{2\left(h_{1,j}r_1+h_{2,j}r_2\right)}{\left(r_2^2-r_1^2\right)}+\frac{2k_{z,j}}{\Delta z_j^2}+\frac{2k_{2,j}}{r_1^2+\frac{1}{2}\left(\frac{r_3-r_2}{2}\right)^2}\right]\left(\frac{\Delta t}{\rho_{2,j}C_{p_{2,j}}}\right) \tag{25}$$

$$C_{2,j}=-\frac{k_{z,j}}{\rho_{2,j}C_{p_{2,j}}}\left(\frac{\Delta t}{\Delta z_j^2}\right) \tag{26}$$

$$D_{2,j}=T_{2,j}^t+\left[\frac{2h_{1,j}r_1T_{1,j}^t+2h_{2,j}r_2T_{3,j}^t}{r_2^2-r_1^2}+\frac{2k_{2,j}\left(T_{1,j}^t+T_{3,j}^t\right)}{r_1^2+\frac{1}{2}\left(\frac{r_3-r_2}{2}\right)^2}-\frac{k_{2,j}\left(T_{3,j}^t-T_{1,j}^t\right)}{\left(\frac{r_3+r_2}{2}\right)\left(r_1^2+\frac{r_3-r_2}{2}\right)}\right]\left(\frac{\Delta t}{\rho_{2,j}C_{p_{2,j}}}\right) \tag{27}$$

Annulus Region

In the annulus region, cold water is injected and circulated, which results in a circulation loop similar to drilling process. The governing equation is still applicable, but this region needs to be divided into two sub-regions (the injection pipe and the annulus space) to accurately characterized the heat transfer behavior and temperature profile. The fluid flow and heat transfer process in the sub-region of injection pipe is an opposite-direction-process of fluid and heat behavior in the tubing, which can be characterized by the same equations in region 1 in reverse directions. For the annulus space, the governing equation and boundary conditions are,

$$\rho_3 C_{p3}\left(\frac{\partial T_3}{\partial t}+v_z\frac{\partial T_3}{\partial z}\right)=\frac{k_r}{r}\frac{\partial T_3}{\partial r}+k_r\frac{\partial^2 T_3}{\partial r^2}+k_z\frac{\partial^2 T_3}{\partial z^2} \tag{28}$$

$$-k_2\left(\frac{\partial T_2}{\partial r}\right)_{r=r_2}=h_2\left(T_2-T_3\right) \tag{29}$$

$$-k_3\left(\frac{\partial T_3}{\partial r}\right)_{r=r_3}=h_3\left(T_4-T_3\right) \tag{30}$$

And solve for corresponding A, B, C and D,

$$A_{3,j} = -v_{z,j}\left(\frac{\Delta t}{2\Delta z_j}\right) - \frac{k_{z,j}}{\rho_{3,j}C_{p_{3,j}}}\left(\frac{\Delta t}{\Delta z_j^2}\right) \tag{31}$$

$$B_{3,j} = 1 + \left[\frac{2\left(h_{2,j}r_2 + h_{3,j}r_3\right)}{\left(r_3^2 - r_2^2\right)} + \frac{2k_{z,j}}{\Delta z_j^2} + \frac{2k_{r,j}}{\left(\frac{r_3 - r_2}{2}\right)^2}\right]\left(\frac{\Delta t}{\rho_{3,j}C_{p_{3,j}}}\right) \tag{32}$$

$$C_{3,j} = -v_{z,j}\left(\frac{\Delta t}{2\Delta z_j}\right) + \frac{k_{z,j}}{\rho_{3,j}C_{p_{3,j}}}\left(\frac{\Delta t}{\Delta z_j^2}\right) \tag{33}$$

$$D_{3,j} = T_{3,j}^t + \left[\frac{2h_{2,j}r_2T_{2,j}^t + 2h_{3,j}r_3T_{4,j}^t}{r_3^2 - r_2^2} + \frac{k_{3,j}\left(T_{2,j}^t + T_{4,j}^t\right)}{\left(\frac{r_3 - r_2}{2}\right)^2} + \frac{k_{3,j}\left(T_{4,j}^t - T_{2,j}^t\right)}{\left(r_3 - r_2\right)\left(r_2 + \frac{r_3 - r_2}{2}\right)}\right]\left(\frac{\Delta t}{\rho_{3,j}C_{p_{3,j}}}\right) \tag{34}$$

It is worthy to be noticed that, the TEGs are installed on the outer surface of tubing and belong to this region, therefore, the effect of TEG on temperature distribution should be considered in this region. TEG under temperature differences will result in heat conduction from hot side to cold side and Joule heating by heat-electricity conversion. To include these effects into temperature distribution, a parameter named "effective thermal conductivity" of TEG (Baranowski et al., 2013) is introduced to encompass the overall heat transfer phenomena. The effect of TEG on heat transfer could be embodied by replacing the thermal conductivity by the effective thermal conductivity. The expression of effective thermal conductivity is

$$k_{eff} = \frac{kT_h\left(1 + zT + \sqrt{zT + 1}\right)}{2\left(T_h - T_c\right)}\left[1 - \left(\frac{T_h}{T_c}\right)^{\beta}\right] \tag{35}$$

$$\beta = \frac{2 - 2\sqrt{zT + 1}}{zT} \tag{36}$$

where T_h and T_c are the temperature values at hot side and cold side, respectively, and k is the thermal conductivity of the thermoelectric material. zT is the dimensionless figure of merit, standing for the ability of a given material to efficiently produce thermoelectric power as

$$zT = \frac{\alpha^2}{k\sigma}\frac{T_h + T_c}{2} \tag{37}$$

where σ is the thermal conductivity and electrical resistivity of the thermoelectric material.

Casing Wall, Cement and Formation Region

The regions of casing wall, cement and formation can be treated as a whole and be solved using same equations because the heat transfer behavior in these regions is only in form of heat conduction, and the governing equation can be simplified as,

$$\rho_4 C_{p4}\left(\frac{\partial T_4}{\partial t}\right) = \frac{k_r}{r}\frac{\partial T_4}{\partial r} + k_r\frac{\partial^2 T_4}{\partial r^2} + k_z\frac{\partial^2 T_4}{\partial z^2} \tag{38}$$

The temperature continuity at the contacting surfaces of casing wall/cement and cement/formation could generate the boundary conditions for each region, and boundary conditions and the above equation could be used to obtain the expression of A, B, C and D in each region separately.

Overall Heat Transfer Coefficient

The heat convection between the flowing fluid (in tubing and in annulus) with the pipe wall (tubing wall and casing wall) can be characterized using convective heat transfer equation with respect to convective heat transfer coefficient, *h*. This coefficient is calculated based on Nusselt number, Nu, and hydraulic diameter, D_h, with the relationship of,

$$Nu = \frac{h}{k} D_h \tag{39}$$

Nusselt number can be determined by the flow regimes in pipe and annulus by corresponding equations in Table 3.

Table 3: Equations of Nusselt number under different conditions

	Fluid flow in pipe	Fluid flow in annulus
Laminar flow	$Nu = 4.364$ (40)	$Nu = 1.86\left(\frac{\mathrm{Re}\cdot \mathrm{Pr}\cdot D}{L}\right)^{\frac{1}{3}}\left(\frac{\mu_b}{\mu_s}\right)^{0.14}$ (41) $\mathrm{Pr} = \frac{\mu}{k} C_p$ (42) $\mathrm{Re} = \frac{\rho v D}{\mu}$ (43)
Turbulent flow	$Nu = \frac{\left(\frac{f}{8}\right)(\mathrm{Re}-1000)\mathrm{Pr}}{1+12.7\left(\frac{f}{8}\right)^{0.5}\left(\mathrm{Pr}^{\frac{2}{3}}-1\right)}$ (44) $f = \left(0.79\ln(\mathrm{Re})-1.64\right)^{-2}$ (45)	